5.1 FIRST EXTENSIVE WHITECAP DATABASE AND ITS USE TO STUDY WHITECAP FRACTION VARIABILITY

Magdalena D. Anguelova, Michael H Bettenhausen, William F. Johnston, Peter W. Gaiser

Remote Sensing Division, Naval Research Laboratory, 20375, Washington DC, USA
Telephone: 202-404-6342; E-mail: maggie.anguelova@nrl.navy.mil

1. INTORUDCTION

Oceanic whitecaps manifest the breaking of wind-driven water waves with air entrainment. They alter the ocean surface albedo and roughness and produce bubbles, sea spray and sea-spray aerosols. Through these processes, breaking waves affect the remote sensing of surface wind vector (Yueh et al., 1999), salinity (Camps et al., 2005) and ocean color (Gordon and Wang, 1994) and are involved in the turbulent mixing of the upper-ocean layer (Melville, 1996), planetary heat budget (Fairall et al., 1994), air-sea gas exchange (Wanninkhof et al., 2009), tropical cyclone intensification (Andreas et al., 2008), and aerosol radiative forcing of climate (Lewis and Schwartz, 2004). Whitecap fraction, W, quantifies the area covered with whitecaps and is used as a forcing variable in models and parameterizations of these processes. Traditional photographic measurements of foam fraction have high experimental uncertainty and are not sufficient to build a database necessary to investigate and model the geophysical variability of W.

Within the framework of WindSat mission (Gaiser et al., 2004), Naval Research Laboratory has developed an alternative method of estimating whitecap fraction from satellite-based passive radiometric data (Anguelova et al., 2006). The algorithm relies on changes of ocean surface emissivity at microwave frequencies (6 to 37 GHz) due to presence of sea foam on a rough sea surface.

Here we describe the first extensive database of satellite-based whitecap fraction and additional meteorological and oceanographic data. The database is used to investigate the geophysical variability of whitecaps with correlation and principal component analyses.

2. WHITECAP DATABASE

2.1 Satellite-based Whitecap Fraction

Anguelova et al. (2009) list changes in the algorithm estimating W and the specific features of the satellite-based W values. Briefly, the shortcomings of the feasibility-study algorithm (Anguelova and Webster, 2006) were improved by usage of independent sources for the input variables of the algorithm, physically based models for the emissivity of rough sea surface and emissivity of foam, improved rain flag, and improved atmospheric model necessary for the atmospheric correction.

Validation of the satellite-based whitecap fraction is not straightforward because of different principles of measurement used—optically for virtually all available *in situ* data and radiometrically for satellite-based data—and the lack of sufficient and well-constrained *in situ* values representing wide range of conditions. Preliminary comparisons of satellite radiometric and ship-borne or aircraft-borne photographic values of W show general consistency (Anguelova et al., 2009). But satellite-based W underestimate W predictions from current $W(U)$ parameterizations at high winds and over estimate both $W(U)$ parameterizations and the *in situ* data at low winds. To evaluate the underestimation, more *in situ* data at high winds are necessary. As for the overestimation at low winds, one must recognize that differences may not be due solely to the satellite-based method because extraction of low (less than 10^{-3}%) whitecap coverage values from video records and photographs are expected to have large errors. Collection and comparison of satellite and *in situ* whitecap data for further comparison is ongoing.

Though satellite-based whitecap observations need further development and improvement, the retrieved data are useful for gaining first insights about the variability of the whitecap fraction. Thus, we compiled a whitecap database with the current version of the W estimates. For the W entries, the whitecap database uses all available WindSat orbits (ascending passes) at swath resolution of 50×70 km^2 for 10 GHz and 37 GHz, horizontal polarization (10H and 37H, respectively). The choice of these frequencies is based on the conclusion of Anguelova et al (2009) that W from 10 GHz, similarly to the photographic W data, would capture all active and partially decaying whitecaps, while W from 37 GHz is good in "seeing" even the thinnest decaying foam patches. The H polarization is used because it is more sensitive to changes of wind speed and breaking-wave events than the vertical polarization.

Figure 1 presents daily global map of foam fraction from WindSat data for 1 March, 2007 (orbits 21479 to 21492). From the raw swath resolution, the whitecap fraction data are mapped globally into 0.5°×0.5° grid box. Gridding statistics, including root-mean-square (rms) error, standard deviation and number of points counted, are associated with each grid box.

Gaps in the daily W data are a notable feature in Figure 1. These appear due to using data from

independent sources for W estimates (Anguelova et al, 2006). Matching data from various sources in time and space produces only 4 full orbits, those resulting from match-ups between WindSat and 6-hour analyses of Global Data Assimilation System (GDAS) developed at National Centers for Environmental Prediction (NCEP). The orbits with diamond-shaped chunks result from matching WindSat and QuikSCAT because the ascending passes of the two satellites are in opposite directions. The gaps move from day to day and over a month global coverage is obtained with the caveat that the number of samples at a given point vary from 1 to 23. The gridding statistics saved in our database (Section 2.1) helps identify grid cells with limited sampling due to this issue. As the algorithm for satellite-based whitecap fraction further develops, it is necessary to evaluate pros and cons of using independent data sources in it versus limited sampling resulting from such a choice.

2.2 Additional Variables

Six additional variables from other satellites or global models are matched-up in time and space with the satellite-based whitecap fraction. These are wind speed, U_{10}, from QuikSCAT or SSM/I depending on the chosen matching criterion; wind direction, ϕ, from QuikSCAT; SST, T_s, and air temperature, T_a, at 2 m reference height above the sea surface from GDAS/NCEP; and significant wave height (SWH), H_s, and mean wave period (MWP), T_p, from NOAA/NCEP WAVEWATCH III model (NWW3).

These data are used to derive two additional variables. The difference between the air and sea-surface temperatures, $\Delta T = T_a - T_s$, can be used as a proxy for the atmospheric stability (Kara et al, 2008). We calculate fetch using SWH and wind speed data following Lafon et al (2004) and the references there in,

$$X \propto g\left(H_s/U_{10}\right)^2.$$

Figure 2 shows monthly (March 2006) maps (0.5°×0.5° grid) for H_s (panel a), ΔT (panel b), and X (panel c). Figure 2b documents well the strongly unstable atmosphere ($\Delta T<0$) over the Kuroshio and Gulfstream currents, as well as the stable conditions ($\Delta T>0$) over the Southern ocean, at this time of the year and attests to the usefulness of the compiled database.

The group of environmental variables $x = [U_{10}, H_s, \Delta T, T_s, X, T_p, \phi]$ in this whitecap database represents four major influences on the whitecap fraction, namely, that of the wind speed, the wave field, the atmospheric stability, and the SST.

The wave field is represented with four characteristics and this gives the possibility to investigate which of them is more effective in representing correlation to W. SWH and MWP (H_s and T_p) can be obtained from models or direct observations. Fetch is not currently measured in any general way; instead reports of field campaigns sporadically estimates it if directional wave spectra are measured

and analyzed. Thus X is the most convenient way to evaluate the effect of the wave-field history on the whitecapping when direct measurements are not available. It also offers the possibility to investigate the effectiveness of representing the influences of wind and wave fields on W separately, e.g., using U_{10} and H_s, versus combining them in one variable. Finally, if one is to establish a general method for direct measurement of fetch, wind direction will most certainly figure prominently in such estimation. On this basis we consider ϕ as a proxy for directly-measured, not calculated, fetch.

2.3 Whitecap Database Features

The whitecap database comprises daily 0.5°×0.5° maps (arrays) for 2006. Time resolutions of 3-days, weekly (7-days) and monthly periods are also available. Statistics for whitecap fraction and the additional variables are also saved for each grid box. Abbreviated database of whitecap fraction from 10H and 37H and only 3 additional variables (wind, wind direction, and SST) on 1°×1° grid, daily and monthly, is also archived.

This is the first extensive whitecap database which features collocated, contemporaneous data for whitecap fraction and additional meteorological and oceanographic data covering wide range of conditions over full seasonal cycle.

3. VARIABILITY ANALYSES

Because satellite-based estimates of W contain information for, and are useful in representing, the whitecapping at specific environmental conditions, they are suitable for developing parameterizations of W as a function of as many additional factors as possible. However, while desirable, the development of such parameterizations may not be wise from modeling point of view; a modeler would prefer to use parameterizations with fewer variables to restrict the propagation of their measuring errors in the model. Thus, it is necessary to evaluate the relative contribution of each factor to the W variability and determine which of the additional factors are important in different regions over the globe. We have pursued this using correlation and principal component analyses (CA and PCA, respectively). In these analyses, we use the 0.5°×0.5° gridded data for W and any other variable x in different combinations (details below).

3.1 Correlation Analysis

For each grid box we construct time series for each of the W-x pairs. When monthly-averaged data are used, the time series formed for each grid box comprise up to 12 (but not less than 8) points. If weekly or 3-days temporally-averaged data are used, the time series formed for each grid box have more points, respectively up to 43 or 109. Here we report results for monthly time series.

For each grid box and each W-x pair we find correlation coefficients, r, as a measure of the presence or strength of linear dependence between two variables.

2

If testing shows that the correlation between W and any variable x is statistically significant, we obtained coefficient of determination, r^2. Because r^2 is a measure of the W variation explained by the factor x, choosing in each grid box the factor with the maximum r^2 (after that of U_{10}) gives us the relative importance of each of the considered additional factors to the whitecaps variability. When none of the additional factors shows a statistically significant correlation with the whitecap fraction, the variance of W was ascribed to the wind speed alone. Color-coding each variable x, we construct a map representing the contribution of each factor, besides the wind speed, to the variance of W. The steps in this procedure follow, with some modifications, the work of Kara et al (2007).

3.2 *Principal Component Analysis*

With principal component analysis (PCA, Preisendorfer, 1988), we investigate the change in the variance explained by the first principal component (1st PC) obtained for data sets comprising W and each x (total of 7 data sets). To make sure that the wind speed does not mask fully the variance explained by additional factors, we repeated the PCA for data sets combining W, U_{10}, and one more variable, namely H_s, T_s, ΔT, and X (four data sets). Finally, to evaluate which wave-field characteristic (H_s, T_p, X, or ϕ) is more effective in explaining the W variations, we performed PCA on data sets combining each of these wave-field factors with W and all other effects for which we have data, i.e., U_{10}, T_s, and ΔT (another four data sets). Prior to PCA, all data sets were standardized, i.e., they were modified to data sets with a mean of zero and variance of one (Preisendorfer, 1988, p. 22).

The data used for PCA were daily values for one month. We report results for March 2006 (section 4). To evaluate whether seasonal changes produce different results, we performed PCA on all same data sets described above for August and December 2006. Though the data sets used for CA and PCA differ (i.e., monthly for CA and daily data for PCA), the results of the two analyses complement each other and help reach broader conclusions (Section 4).

4. RESULTS AND DISCUSSION

With the wide range of conditions covered, the whitecap database is well suited to investigate the whitecap spatial and temporal variability (Sections 4.1) and its correlation to various environmental forcing factors (Sections 4.2 and 4.3). CA and PCA were applied to W from 10H and 37H satellite observations, but only the results for W from 10H are shown and discussed here. CA and PCA results for W from 37H lead to the same conclusions as those from 10H.

4.1 *Spatial and Temporal Whitecap Variations*

Figure 3 shows global monthly (March 2006) distribution of whitecap fraction from WindSat measurements at 10H (upper panel) and whitecap fraction obtained from $W(U_{10})$ parameterization (lower panel) (Monahan and O'Muirchaertaigh, 1980). The spatial distributions have similar features but somewhat different magnitudes. The former is expected as satellite-based W values from 10H were found to be the closest to the photographically measured W values (Anguelova et al., 2009). The later points toward more uniform distribution of whitecap coverage from low to high latitudes, a finding which, though not as strongly expressed as in the feasibility study (Anguelova and Webster, 2006), is preserved in the new W estimates and can be plausibly explained. Partially, it could be a consequence of still developing and improving performance of the retrieval algorithm. But it could also represent influences of the additional factors on the whitecapping. For example, the high winds in the Southern ocean are coupled with mostly stable atmospheric conditions in this time of the year (e.g., Figure 2b), low SST which supports increased viscous dissipation, relatively strong Circumpolar current usually aligned with the Westerlies, and highly productive waters which supply higher concentrations of surface active materials. All these additional factors act to suppress the whitecapping, thus the observed lower values for W as compared to those predicted by the wind-speed-only relationship.

Figure 4 presents seasonal changes of the whitecap fraction for 2006 obtained from 37H. Besides the shift of high W values from North to South Hemisphere during boreal and austral winters and springs, note the generally higher W values at 37H than those at 10H. As noted before (Anguelova et al, 2009), this is a consequence of the different sensitivity of these two frequencies to different stages of the whitecap lifetime; 37H detects more foam than 10H because with its thinner skin depth it probes thin decaying patches of foam better than 10H does.

4.2 *Contributing Factors from CA*

The maps in Figure 5 exemplify the correlation between W and U_{10} (panel a), W and ΔT (panel b), and W and X (panel c). The scale for the correlation coefficient in Figure 5a is from 0.8 to 1 clearly demonstrating the well known fact of strong positive correlation between wind and whitecap formation. With a scale for r from -1 to +1, Figure 5b shows strong positive correlation (warm colors) between whitecap fraction and atmospheric stability at low latitudes and strong negative (cold colors) correlation between the two at high latitudes. That is, annual stability conditions at lower latitudes act to increase the whitecap coverage, while the annual stability conditions at higher latitudes could decrease it. In the well known bands of Westerly and Easterly winds, Figure 5c shows strong positive correlation between whitecaps and fetch in areas to which winds blow over long distances (long fetch causes high whitecapping) and in confined basins (e.g., Arabian sea and the Gulf of Mexico) where low whitecapping could be associated with short fetches. Close to large land masses (e.g., east of South America and South Africa), where fetches are still short; strong negative W-X correlation (i.e., short fetch and high

whitecapping) can be explained as a consequence of more frequent breaking of young seas which are undeveloped in areas with short fetches.

The map in Figure 6, constructed with CA (Section 3.1), shows which factor where on the globe contributes the most to the W variance besides the wind speed. Areas marked with green are places where no additional factor has shown statistically significant correlation with W and only wind is important. While at lower latitudes these green places may be result of lack of physical influence of additional factors on W, the green places at high latitudes are most probably due to the sampling issue noted in Section 2.1. Because we use at least 8 points to construct the correlation maps (Section 3.1), there are grid cells where r is not obtained. According to Figure 6, the significant wave height (purple areas) and the fetch (yellow areas) explain most of the spatial variability of W. SST contributes mostly at low latitudes (red places). Air-water temperature differences (magenta) are spread over different places but usually over areas where the atmospheric stability has strong seasonal cycle, e.g., high latitudes and over the Kuroshio and Gulfstream. This map informs us that in developing new parameterizations of whitecap fraction we need to start with wind speed and wave field characteristics and account for the effects of SST and atmospheric stability only in some specific places.

4.3 *Contributing Factors from PCA*

Results of PCA (Section 3.2) are shown in Figure 7. Plotted in the figure are percent variances explained by the 1stPC for seven data sets combining W with each factor x (blue line). After the wind speed, the 1stPC of the [W, H_s] data set explains most of the variance (82%), followed by about 67% variance explained by the 1stPCs of data sets [W, T_s] and [W, ΔT]. These are followed, in decreasing order, by the 1stPCs of the data sets involving ϕ, X, and T_p.

The ranking of the percent variance explained by the 1stPCs associated with H_s, T_s, ΔT, and X when wind speed is also included in the data set is preserved despite slight changes in the absolute values (red symbols in Figure 7). The PCA thus corroborates the result of the CA that the additional factor which influences the variations of the whitecap fraction the most is the wave field.

Regarding SST and the atmospheric stability, two conclusions emerge from the PCA. First, both SST and ΔT have almost the same effect on the W variability. This is useful result because it suggests that we can choose either SST or ΔT to parameterize the variability due to any of them. Because SST is routinely and more accurately measured than T_a (thus ΔT), the choice is obvious. Since the data sets used for PCA are daily data for one month (i.e., relatively small temporal variations), most of the W variance which SST and ΔT explain is associated with their spatial variability from low to high latitudes. The map in Figure 6 shows the regions where seawater and air temperature effects need to be considered.

The second PCA result regarding SST and the atmospheric stability is that the variance they explain is higher than that explained by X (Figure 7). This is in contrast to the results in Figure 6, where X emerges as the second most influential additional factor after H_s. The discrepancy could be due to the representation of monthly (in the case of PCA) versus annual (in the case of CA) temporal variations of the involved variables. Performing CA and constructing maps similar to that in Figure 6 on daily data for several months could give more insights.

PCA applied to the four data sets involving [W, U_{10}, T_s, ΔT] and each of the wave field characteristics (H_s, ϕ, X, and T_p) establishes H_s as the more efficient one because its 1stPC explains the highest variance compared to the variances explained by ϕ, X, and T_p (green symbols in Figure 7). This is in agreement with the results in Figure 6 from CA. PCA of these four data sets also suggests that if measured fetch (represented here by ϕ) is available, it might be more useful in representing the wave field effect on W variability than calculated fetch X. Because presently no specific procedure exist to measure fetch and because various parameterizations exist to calculate X (Lafon et al., 2004), the PCA of these four data sets points that the SWH is more suitable to account for wave field effect on W.

The PCA results for August and December data produce slightly different values but these differences do not change the conclusions above.

Overall, the results of both CA and PCA narrow down the useful additional factors which need to be considered in addition to wind speed to SWH and SST.

5. CONCLUSIONS

Further developments of an algorithm to estimate whitecap fraction from microwave passive observations have produced useful data. With these an extensive database of whitecap fraction and additional variables has been compiled. The database is suitable to investigate spatial and temporal variation of whitecap fraction over the globe. Global spatial distribution of satellite-based values of W differ from those obtained with conventional $W(U_{10})$ relationships. The differences could be explained with the influence of additional meteorological and environmental factors on whitecap formation.

Correlation analysis helps mapping the contribution of various additional factors to the W variance in various geographical regions. Principal component analysis corroborates the results of the correlation analysis and helps narrow the range of additional factors necessary to parameterize W variability. Besides wind speed, wave field—represented with significant wave height—and SST are the factors that need to be considered when parameterizing whitecap fraction.

6. REFERENCES

Andreas, E.L., P.P.G. Persson, J.E. Hare, 2008: A bulk turbulent air-sea flux algorithm for high-wind, spray conditions, *J. Phys. Oceangr.*, **38**, 1581-1596, doi:10.1175/2007JPO3813.1.

Anguelova, M.D., M.H. Bettenhausen, and P.W. Gaiser, 2006: Passive remote sensing of sea foam using physically-based modes. *IEEE International Geoscience and Remote Sensing Symposium* (IGARSS'06), Proceedings, 7, 3676 - 3679.

Anguelova, M.D., J. P. Bobak, W. E. Asher, D. J. Dowgiallo, B. I. Moat, R. W. Pascal, and M. J. Yelland, 2009: Validation of satellite-based estimates of whitecap coverage: Approaches and initial results, January 2009, Proceeding 16th Conference on Air-Sea Interaction, (ams.confex.com/ams/89annual/techprogram/paper_143665.htm)

Anguelova, M.D., and F. Webster, 2006: Whitecap coverage from satellite measurements: A first step toward modeling the variability of oceanic whitecaps. *J. Geophys. Res.-Oceans*, 111, C03017, doi:10.1029/2005JC003158.

Camps, A., et al., 2005: The emissivity of foam-covered water surface at L-band: theoretical modeling and experimental results from the FROG 2003 field experiment, *IEEE Trans. Geosci. Remote Sens.*, **43**,925-937.

Fairall, C., J. Keppert, and G. Holland, 1994: The effect of sea spray on surface energy transport over the ocean, *Global Atm. And Ocean Sys.*, *2*, 121-142.

Gaiser, P., et al., 2004: The WindSat spaceborne polarimetric microwave radiometer: sensor description and early orbit performance**,** *IEEE Trans. Geosci. Remote Sens.*, vol. 42, pp. 2347 – 2361.

Gordon, H. R. and M Wang, 1994: Influence of oceanic whitecaps on atmospheric correction of ocean-color sensors, *Appl. Opt*, vol. 33, no. 33, pp. 7754-7763.

Kara, A. B., H. E. Hurlburt, and W.-Y. Loh, 2007: Which near–surface atmospheric variable drives air–sea temperature differences over the global ocean?, *J. Geophys. Res.*, 112, C05020, doi:10.1029/2006JC003833

Kara, A. B., A. J. Wallcraft, and M. A. Bourassa, 2008: Air-sea stability effects on the 10 m winds over the global ocean: Evaluations of air-sea flux algorithms, *J. Geophys. Res.*, 113, C04009, doi:10.1029/2007JC004324.

Lafon, C., J. Piazzola, P. Forget, O. le Calve, and S. Despiau, 2004: Analysis of the variations of the whitecap fraction as measured in a coastal zone, *Boundary-Layer Meteorol.*, *111*, 339-360.

Lewis E. R. and Schwartz S. E., 2004: *Sea Salt Aerosol Production: Mechanisms, Methods, Measurements, and Models -- A Critical Review*, Geophysical Monograph Series Vol. 152, American Geophysical Union, Washington.

Melville, W.K., 1996: The role of surface-wave breaking in air-sea interaction, *Annu. Rev.Fluid Mech.*, 28, 279-321.

Monahan, E., and I. G. O'Muircheartaigh, 1980: Optimal power-law description of oceanic whitecap coverage dependence on wind speed. *J. Phys. Oceanogr.*, 10, 2094–2099.

Preisendorfer, R. W., 1988: *Principal component analysis in meteorology and oceanography*, Ed. C.D. Mobley, Elsevier, New York.

Wanninkhof, R., W.E. Asher, D.T. Ho, C. Sweeney, W.R. McGillis, 2009: Advances in Quantifying Air-Sea Gas Exchange and Environmental Forcing, *Annu. Rev. Mar. Sci.*, **1**, 213-244, doi:10.1146/annurev.marine.010908.163742.

Yueh, S.H., W.J. Wilson, S.J. Dinardo, and F.K. Li, 1999: Polarimetric microwave brightness signatures of ocean wind directions, *IEEE Trans. Geosci. Rem. Sens.*, vol. 37, pp. 949-959.
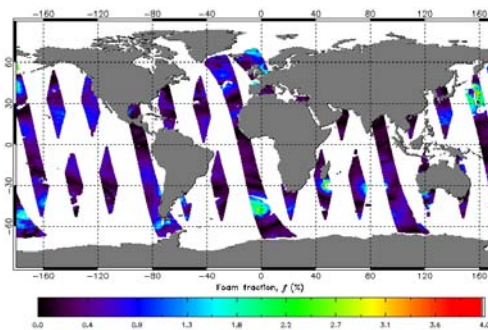
Figure 1 Foam fraction *W* (in %) from satellite data at 10 GHz, H pol. Daily map for 1 March 2007 (orbits 21479 to 21492), swath resolution.
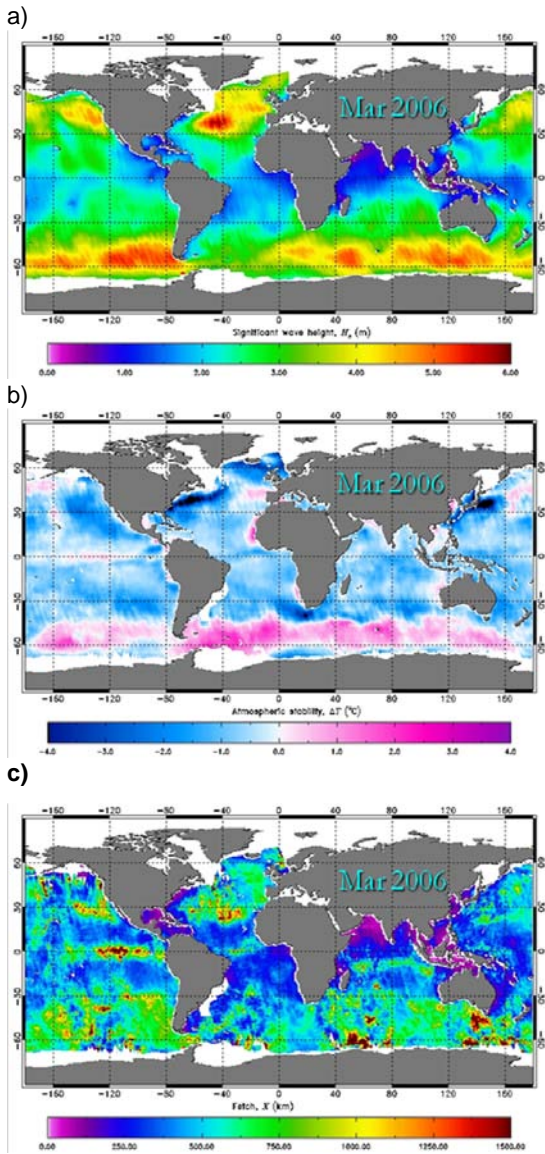
a)

b)

c)

Figure 2 Monthly (March 2006) maps (0.5°×0.5° grid) for significant wave height H_s (panel a) obtained from NOAA/NCEP wave model (NWW3), air-water temperature difference, ΔT (panel b), and fetch X (panel c).
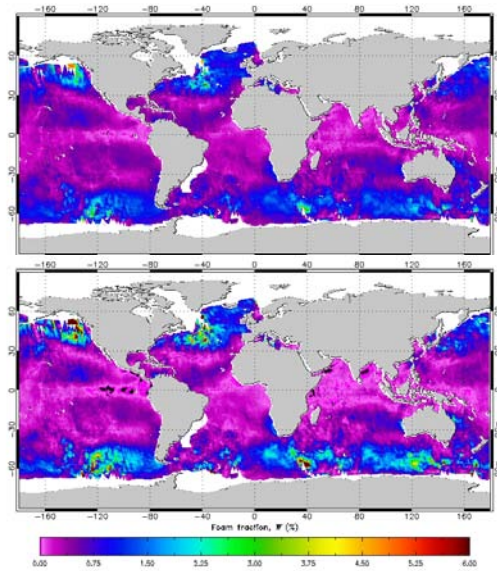

Figure 3 Global monthly (March, 2006) distribution of whitecap coverage from WindSat measurements at 10 GHz, H pol. (10H, upper panel) and $W(U_{10})$ model of Monahan and O'Muirchaertaigh (1980) (lower panel).
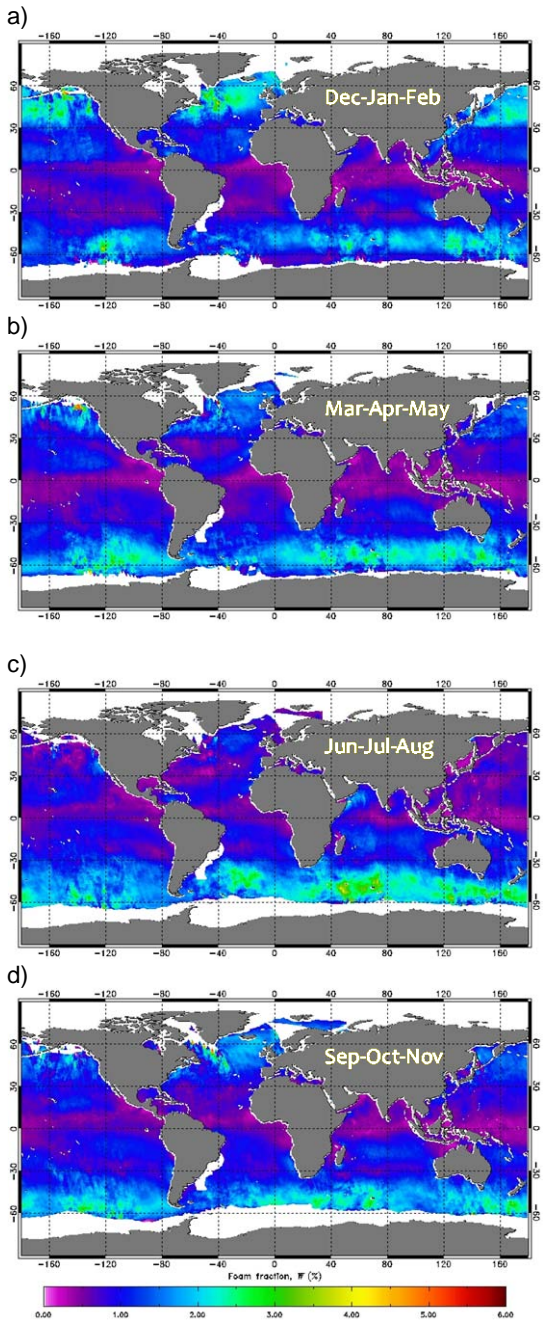
a)

b)

c)

d)

Figure 4 Global seasonal distribution of whitecap coverage for 2006 from WindSat measurements at 37 GHz, H pol.
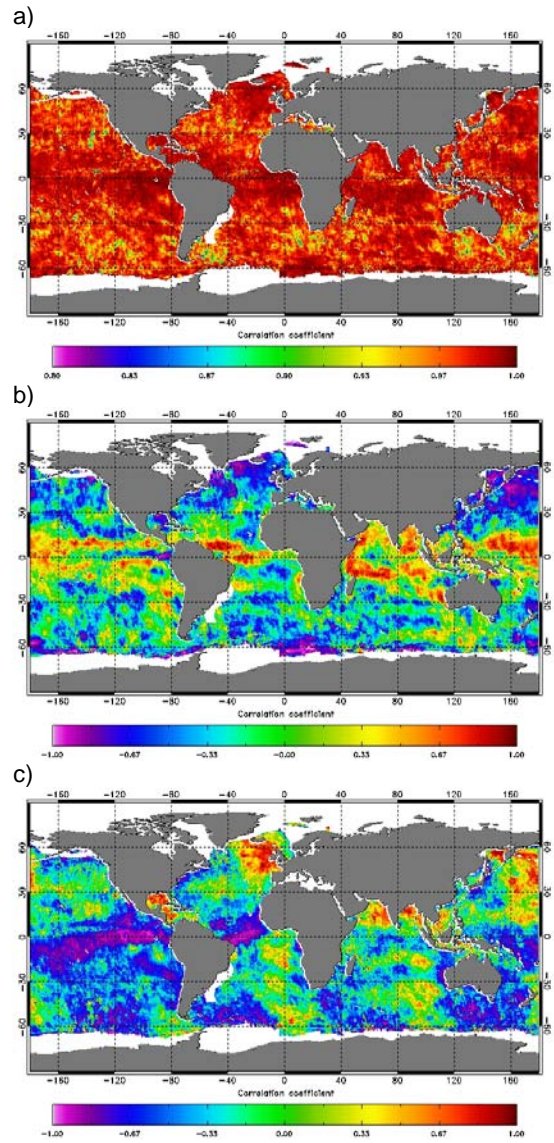
a)

b)

c)

Figure 5 Correlation maps for W and U_{10} (panel a), W and ΔT (panel b), and W and X (panel c). In (a) the color bar range is from 0.8 to 1; in (b) and (c) the color bar range is from -1 to 1.
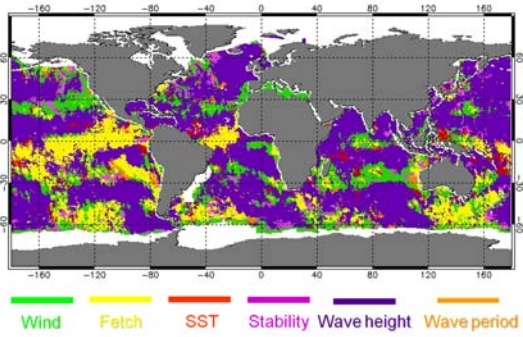
Figure 6 Contribution of various factors to the variance of whitecap fraction. Green is for wind speed, yellow for fetch, red for SST, magenta for atmospheric stability, purple for significant wave height, and orange for mean wave period.
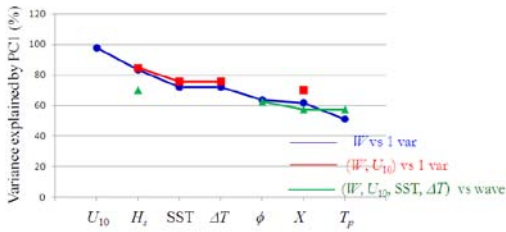

Figure 7 Percent variances explained by the 1st PC for data sets combining W with various factors $x = [U_{10}, H_s, T_s, \Delta T, \phi, X, T_p]$.